Date	31 October 2022	Ver	1.0
Ref	esa10475-cots-detector-final	Sign-off	Jann Eike KRUSE

Title	**Sub-Activity #2: “COTS SiPM Detector” – Final Report**

Scope of this document

In this document, we summarise and discuss the experiments, achievements and measurement results obtained throughout this sub-activity.

This Final Report focuses on the most relevant conclusions as well as on all the activities of the second half of the roadmap, covering the days from 15 August until end of September.

A separate report, published previously with Reference *esa10475-cots-detector-midterm*, covers the first half of the sub-action, reporting on the activities and achievements from the beginning of July until middle of August.

Summary

Onsemi silicon photomultiplier (SiPM) sensors, also known as multi-pixel photon counter (MPPC) devices, can indeed lend themselves very well as suitable choice for a low-cost consumer/off-the-shelf laser downlink receiver.

They provide both the photo-sensitivity in the few-nanowatt range and the temporal response in the few-nanosecond range, necessary to receive currently deployed laser downlinks in the visible and near-IR spectral range from LEO at speeds of up to a 100 Mbps and possibly beyond.

Discussion

Synopsis

We have been able to measure a pseudo-random bitstream (pattern: 1001110_b) at 50 Mbps (20 ns / bit) at an average received power of about $P_{AVE} \approx 100$ nW, as well as a somewhat noisy but still decodable signal even at $P_{AVE} < 20$ nW, as illustrated in Figure 1.

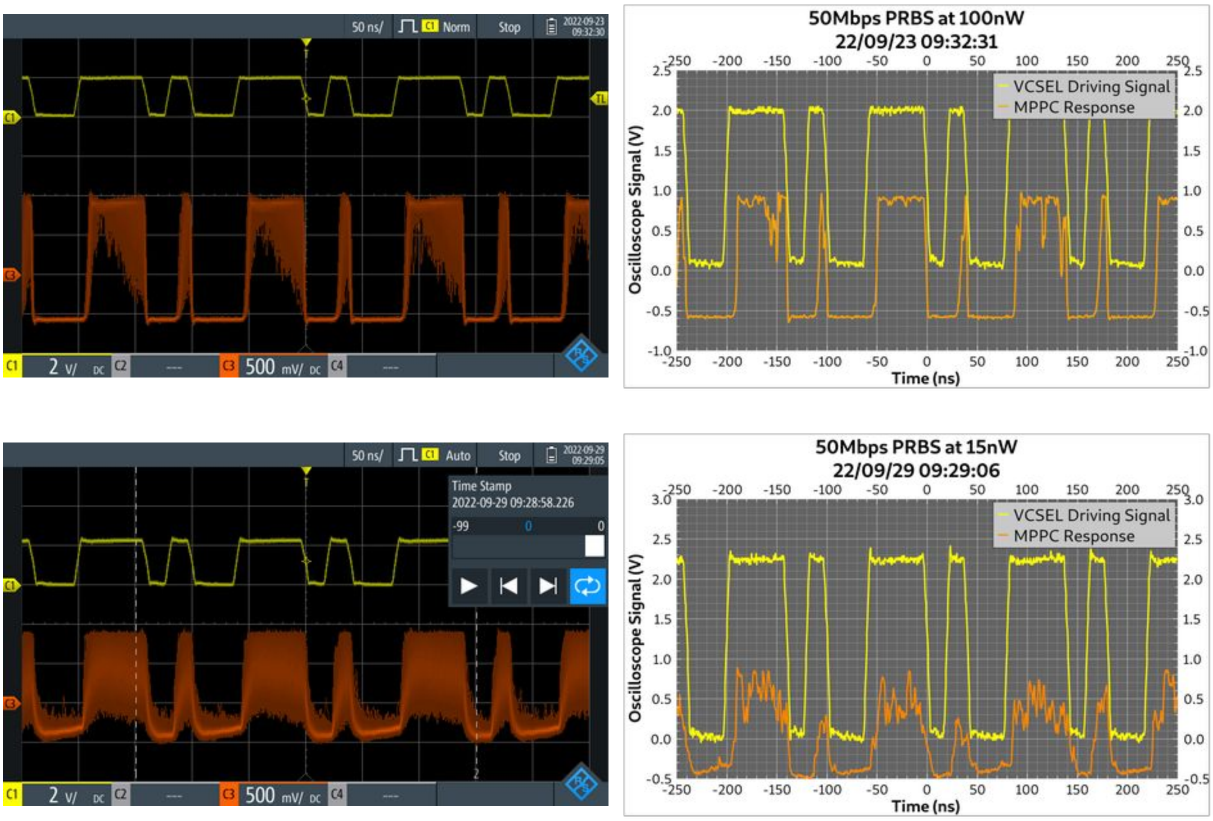

Figure 1: Screenshot and data plots of a 7-bit repeating PRBS at 50 Mbps.
Top row: P_{AVE} = 100 nW, Bottom row: P_{AVE} = 14.3 nW
C1 (yellow) : Signal sent to VCSEL
C3 (orange) : Signal received from MPPC (after two-stage aplification)

To compare this, for example, with the expected power received from a satellite in LEO ($d \approx 500$ km), equipped with the OSIRISv2 transmitter (providing a $P_{Peak} \approx 1$ Watt and a beam divergence of 1.2 mrad FWHM), and an assumed 90% loss through atmosphere and optics, at the sensor of a 12"-diameter telescope from a 50% duty cycle bit stream, one can expect about 15 nW.

Received signal characteristics

Low-intensity Threshold

A critical value for the lowest light intensity threshold, below which data can not any more be accurately decoded, is determined by the signal-to-noise ratio. The noise in this test-bed setting is defined by the dark count of the SiPM device. The signal in this test-bed setting is the photon count during a logical bit of the bit stream, determined by the level of the driving signal to the VCSEL, the optics and the neutral-density filter attenuators. For the error ratio to be sufficiently low, the photon count should be sufficiently high, so that during the vast majority of the bits in the bit stream the photon count is significantly higher than the dark count. From the lowest-intensity measurements taken with the current setup, illustrated in Figure 2, the low-intensity threshold appears to be in the range of 1 nW to about 10 nW, depending or the sophistication of the post processing of the signal.

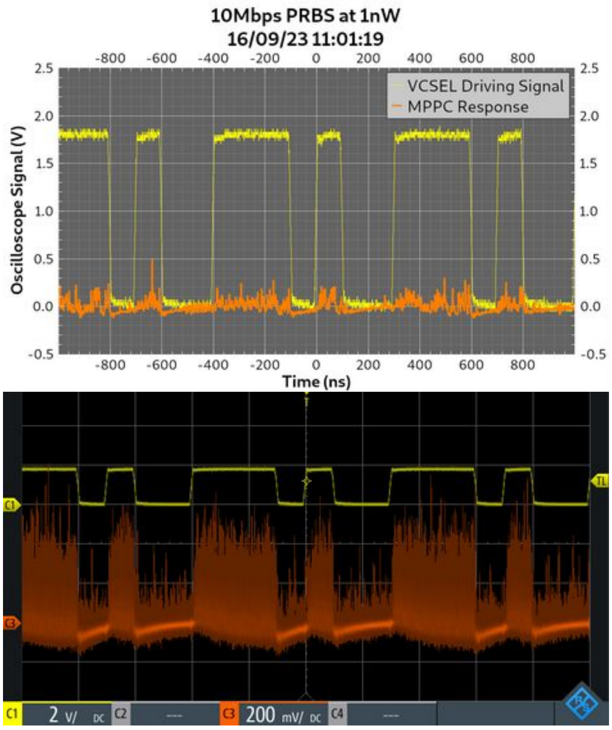

Figure 2: 10 Mbps PRBS at P_{AVE} = 1 nW

This critical level of illumination ($P_{min} \approx 10$ nW) can be compared to the expected level of illumination ($P_{RX} \approx 25$ nW) in a real-world setting, taking for example the OSIRISv2 payload in LEO:

Given a transmission power of $P_{TX} = 1$ W and a FWHM half angle of the transmitting beam divergence of $\theta_{FWHM} = 0.6$ mrad and the distance between the transmitter and the receiver of $d = 500$ km, then the beam radius at the receiver can be approximated as $r_{RX} \approx \theta \cdot d \approx 300$ m, i.e. a FWHM beam diameter of about 600 m. For sake of simplicity, we shall approximate this as flat-top beam, i.e. as homogeneously illuminated area of 600 meters diameter.

A 12-inch telescope with approximately 0.3 m aperture corresponds to $0.5 \cdot 10^{-3}$ of that beam diameter, i.e. $(0.5 \cdot 10^{-3})^2$ of area. Thus $0.25 \cdot 10^{-6}$ of the energy reaching earth will enter the 12” telescope. Approximately 90% of the photons are lost due to atmospheric absorption, scattering and attenuation in the receiver’s optics, which makes for another factor of 10, resulting in a factor of $25 \cdot 10^{-9}$, i.e. 25nW at the focal point of the receiver, given a 1 W transmitter.

Amplifier Saturation

The output of the two-stage pre-amplifier (two of Thorlabs ZFL1000NL+) shows a saturation at an upper level around 900 mV, evident for example in Figure 1, during a “logic high” signal from bit streams with average power above about $P_{RX} \gtrsim 50$ nW. Due to the frequency response of the pre-amplifier, the low frequencies and the DC component is missing. Thus, the “logic low” does not reside at 0 mV, but at position of -0.6V, which results in a peak-to-peak voltage of 1.5 V_{PP} at a 50Ω impedance, corresponding to a +7.5dBm total output signal.

Microcell Depletion

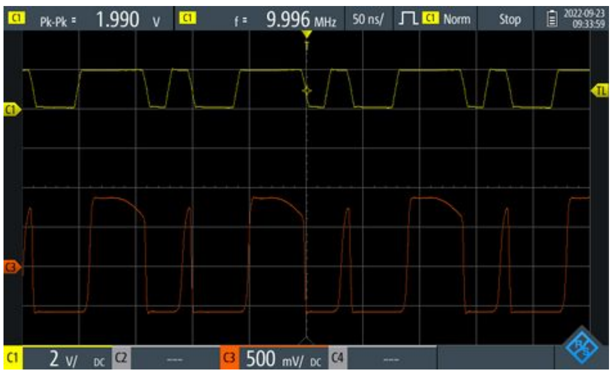

Figure 3: Averaged signal, 50Mbps, 100nW.

As can be seen especially in the top-right section of Figure 1, the signal has a tendency to drop when illuminated continuously at 100 nW. This is likely due to the fact that a significant portion of the microcells have discharged but have not yet recovered and recharged. When recording the average over many waveforms, shown in Figure 3, after about 20 ns of illumination, the average signal starts to drop by ~17% during the following 20 ns from originally 1.45 V to 1.20 V.

For this reason, we recommend that the encoding for the **bitstream should be run-length limited** to minimize the effect of microcell depletion.

Rising Edge Delay and Phase Shift

There is a significant delay of about $\Delta t_{\mathrm{Rise}} \approx 10$ ns between the rising edge of the VCSEL driving signal and the rising edge of the signal received from the SiPM visible in Figure 3, which can be attributed almost entirely to the on-switching time of the VCSEL device, as will become evident in the following. On the other hand, the falling edge has a much lower delay of about $\Delta t_{\mathrm{Fall}} \approx 2$ ns, which may be partially attributed to the of-switching time of the VCSEL (discharge time of the PN junction) and partially to the delay inside the 2-stage signal amplifier. For comparison, a 1 $V_{\mathrm{Pk\text{-}Pk}}$ sinusoidal modulation on top of a 2 V bias suffers a delay of about 4 ns between VCSEL driving signal and SiPM signal, as shown in Figure 4.

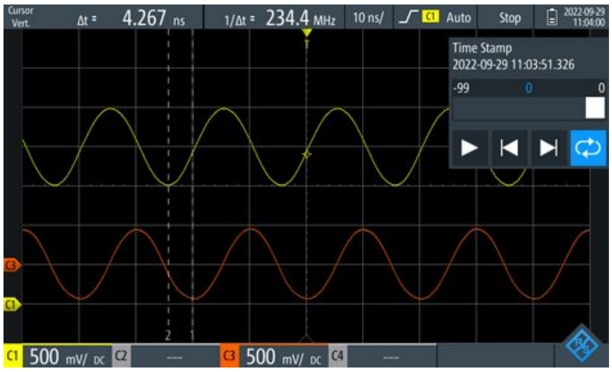

Figure 4: Phase shift between sinusoidal VCSEL driving signal and received SiPM signal

Figure 5 shows that overdriving the VCSEL with a short pulse of 3.6 V from a pre-charged level at 1.5V results in even less than $\Delta t_{\mathrm{Rise}} < 3$ ns delay between rising edge of VCSEL driving signal to rising edge of SiPM response. This points to the fact that the $\Delta t_{\mathrm{Rise}} \approx 10$ ns for a simple on-off VCSEL driving signal is mostly accounted for by the time needed for the VCSEL to start lasing.

Figure 5: Delay between overdriven VCSEL and received SiPM signal

Achievements

Additionally to the achievements already mentioned in the Mid-Term Report, we have proceeded in characterizing the light source more accurately as well as in characterizing the detector, using illumination patterns comparable to those found in the application setting, when used as low-cost COTS ground-station receiver for laser light signals from a low-earth orbit transmitter. In the following sections we describe the experiments and measurements taken.

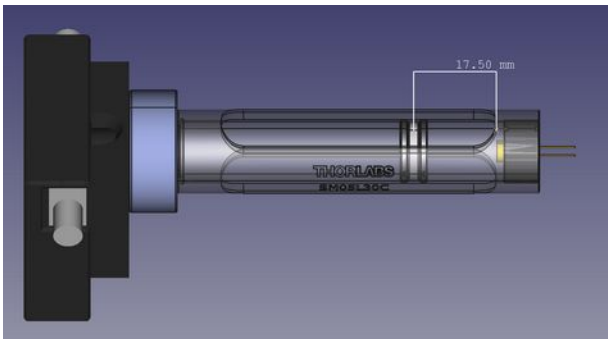

Figure 6: Optical beam path without pinhole without neutral density filter. (3D CAD)

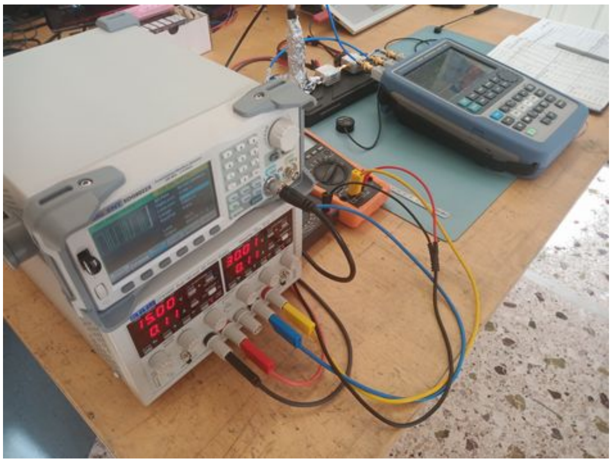
Figure 7: Experiment setup showing the function generator, power supply and oscilloscope.

Change of Optical Setup due to Instability

When measuring the received power at the focal plane of the optical setup, i.e. at the position where the SiPM sensor would be localized, with a NIST-traceable calibrated power meter, we realized that the measured power values with various neutral-density filters were neither consistent nor repeatable. After further investigation, we concluded, that the ⌀200µm pinhole had some play inside of its mount, which resulted in different parts of the laser beam passing through the pinhole depending on the exact position of the pinhole with respect to the laser beam.

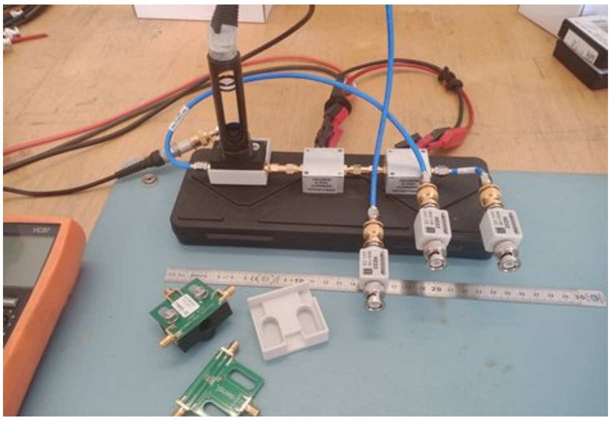
Figure 8: Experiment setup showing the lens tube the pre-amplifiers, SiPM modules and 3D-printed lens-tube adapter and cradle.

Since the pinhole was an optional element in the optical beam path, we chose to **remove the pinhole**, after which the stability of the received power was consistent and repeatable within the expected accuracy and tolerances. The new experiment setup is depicted in Figures 6-8.

Update of Signal Source Characterization

We measured again the focal image, in order to profile the intensity distribution on the SiPM sensor, without pinhole. It turned out that **the laser beam was focused equally well** compared to the focal spot obtained with pinhole. We measured a nearly Gaussian intensity distribution with about ⌀120µm FWHM, as illustrated in Figure 9.

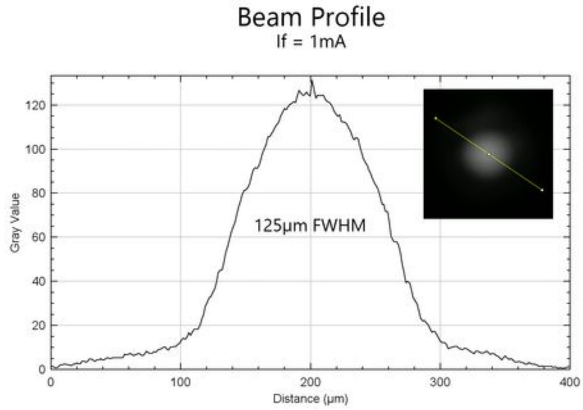

Figure 9: Beam profile and focal image (inset)

Additionally, we could now accurately measure the received power at the focal plane for various VCSEL forward current settings, both without and with neutral-density filters of various nominal optical densities of OD3, OD4, OD5, and OD6, i.e. with nominally 30, 40, 50, and 60 dB attenuation, respectively.

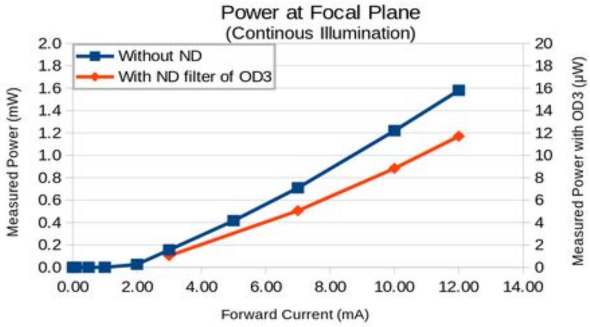

Figure 10: Received power for various VCSEL forward currents, with OD3 neutral density filter (red line, right-side Y axis) and without filter (blue line, left-side Y axis).

This resulted in a new *I/P* curve for the VCSEL shown in Figure 10, as well as in more accurate attenuation values for the neutral density filters at 850nm, shown in Table 1.

Nominal optical density	Measured attenuation
OD3	-21.5 dB (±0.2dB)
OD4	-27.5 dB (±0.3dB)
OD5	-34.7 dB (±0.3dB)
OD6	-32.9 dB (±0.3dB)

Table 1: Measured attenuation of neutral density filters

Detector Signal Acquisition

With the knowledge of laser beam profile, accurate intensity measurements and the actual attenuation of the neutral density filters at 850nm, we commenced to record the signal of the SiPM at various speeds and optical signal intensities. We recorded pseudo-random bit streams at BAUD rates of 10 Mbps, 50 Mbps and 100 Mbps, with average light intensities from 0.25 nW up to 100 nW. For the sake of simplicity, repeatability and in order to be able to easily average over multiple acquisitions, we chose to use a repeating 7-bit pattern, which corresponds to a binary pattern of 1001110_b. Additionally, we recorded a near-sinusoidally amplitude-modulated signal at 50MHz.

The most relevant results these experiments are presented in the Discussion section, while all data, screenshots, photos and relevant notes from the laboratory log book can be found in the Annex, i.e. in the attached ZIP archive.

Divergence from Road-Map

As already mentioned in the Mid-Term Report, we have skipped the production of the VCSEL-driver PCB, because the available arbitrary-function generator (Siglent SDG6022X) was sufficient to drive the VCSEL at the amplitudes and speeds described in the Achievements section.

Annex

List of folders and files in the attached ZIP archive:

- **1. Acquisition**

  BOM.md
  Markdown-formatted file listing all parts purchased for this project

  - **Invoices**
    Folder containing all invoices for the parts listed in the BOM.md file

- **2. PCB**

  [empty]

- **3. 3D-Printed Parts**
  Folder containing 3D Design files for the 3D-printed adapters to fit the OnSemi SensL SiMP break-out boards with SMA connectors to the THORLABS ½-inch lens tubes as well as a cradle to support the board and to isolate it optically and electronically.

  - **1mm-sensor adapter (with viewport)**

    MicroRB_case_2.2_1mm_window.FCStd
    FreeCAD-format 3D CAD design file

    MicroRB_case_2.2_1mm_window.stl
    STL-format triangulated 3D shape

    MicroRB_case_2.2_1mm_window.gcode
    G-Code CNC file for controlling a LulzBot TAZ6 3D printer.

  - **1mm-sensor adapter (without viewport)**

    MicroRB_case_2.2_1mm.FCStd
    FreeCAD-format 3D CAD design file

    MicroRB_case_2.2_1mm.stl
    STL-format triangulated 3D shape

  - **6mm-sensor adapter (without viewport)**

    MicroRB_case_2-2_6mm.FCStd
    FreeCAD-format 3D CAD design file

MicroRB_case_2-2_6mm.stl
STL-format triangulated 3D shape

- **PCB Cradle**

  PCB cradle.FCStd
  FreeCAD-format 3D CAD design file

  PCB cradle.stl
  STL-format triangulated 3D shape

- **4. Optical Path Assembly**

  Optical Assembly (with PM) V2.FCStd
  FreeCAD file showing the improved version assembly with Power Meter

  Optical Assembly (with SiPM) V2.FCStd
  FreeCAD file showing the improved version of the assembly with SiPM PCB, 3D-printed adapter and protective base

- **5. Signal Path Assembly**

  SignalAssembly-SiPM.sch
  KiCAD schematic for the signal assembly
  with low-noise high-speed amplifier for pulse measurements

  SignalAssembly-SiPM.pdf
  PDF plot of the above schematic

- **6. Light source characterization**

  Beam Divergence (with pinhole).ods
  Spreadsheet containing the beam diameters at different distance from the 0.2mm pinhole

  Beam Divergence (no pinhole).ods
  Spreadsheet containing the beam diameters at different distance from the VCSEL.ods

  - Focus images (with pinhole)
    Folder containing images of the focus at different laser intensity and different exposure times.

- Focus images (no pinhole)
  Folder containing images of the focus at different laser intensity and different exposure times.
- Beam Profile (with pinhole).png
  Focus image and cross-section plot to determine the FWHM of the focal spot at the image plane

  Beam Profile (no pinhole).png
  Focus image and cross-section plot to determine the FWHM of the focal spot at the image plane

  OPV310 - IV Curves.ods
  Spreadsheet containing I/V data for three specimens of OPV310 VCSELs

  Power measurement at focal plane (no pinhole).ods
  Spreadsheet containing the measured power at various forward current values and a plot with linear fit

  Power measurement at focal plane (no pinhole with ND filters).ods
  Spreadsheet containing the measured power at various forward current values and a plot with linear fit

- **7. Detector characterization**

  MicroFC-SMA-10010-GEVB I-V curves.ods
  Spreadsheet containing I/V data for the 1mm sensor and fit to determine breakthrough voltage and optimal overvoltage.

  - Oscilloscope recordings
    Folders with screenshots and data from the oscilloscope, measuring the SiPM response at various patterns, BAUD rates and receiver intensities

- **8. Documentation**

  Quick-Start Manual.odt
  Instructions on how to set up the SiPM sensor.

Quick-Start Manual.pdf
PDF version of the above document.

- Data Sheets
  Folder containing data sheets of the SiPM, the VCSEL and the pre-amplifier.

- **9. Management**

  Final Report.odt
  This document

  Final Report.pdf
  This document in PDF format